Sensors and Materials, Vol. 8, No. 1 (1996) 013–022
MYU Tokyo

S & M 0221

Two-Dimensional Analysis of Incompressible Viscous Flow in Ducts Using a Rotated Difference Scheme

Dravia Thangaraj and Arokia Nathan

Department of Electrical and Computer Engineering
University of Waterloo, Waterloo, Ontario
N2L 3G1, Canada

(Received May 4, 1995; accepted September 12, 1995)

Key words: reattachment length in flow channels, Navier-Stokes equation, rotated finite difference scheme

We present two-dimensional numerical solutions to the Navier-Stokes equations for steady, incompressible viscous flow in ducts using a rotated finite difference scheme. To illustrate the numerical scheme, a simple flow channel geometry of small enlargement angle is considered. We compute the flow character along with the reattachment lengths for the range of flow velocities of interest to microflow sensor applications.

1. Introduction

The output response and sensitivity of microflow sensors are determined by the nature of fluid flow (laminar or turbulent) the sensor detects in a duct or a flow channel. The flow can create a recirculation (or vortex) region with length depending on inlet velocity, kinematic viscosity of the fluid and channel geometry. Thus, the ability to predict the character of flow for a given fluid kinematic viscosity and range of inlet velocities is critical to the geometrical/structural design of the flow channel, which is often an integral part of the microsensor package.[1,2] Likewise if the flow channel suffers from dimensional constraints, knowledge of the exact velocity distribution in the channel can aid in calibration/compensation of the microsensor output response.

The flow behavior is governed by the Navier-Stokes equations of fluid motion that are nonlinear and impossible to solve analytically for particular problems. Various numerical

methods have been proposed to solve the Navier-Stokes equations.[3–8] Considerable numerical and experimental work has been reported[7–9] for the reattachment lengths for flows past circular cylinders. It is generally observed that the reattachment length varies linearly with the Reynolds number for low flows (Reynolds number ≤ 100). The laminar flow behavior for special ducts, such as a 'backward facing step,' has been well studied by various numerical methods.[6] Here the reattachment length is observed to be strongly dependent on the numerical method used in discretizing the governing equations. For Reynolds number of the order of 500, the efficiency of the numerical discretization depends on the type of discretization scheme used for the convective derivative term. Many upwind methods have been proposed to deal with this issue. Depending upon the discretization, the schemes may add numerical dissipation in the direction of the streamline or perpendicular to it.

In this work, a rotated finite difference scheme, which takes into account the local characteristics of the streamline, is employed to simulate the two-dimensional, steady-state, incompressible viscous fluid flow in a duct. Ducts, for which the cross-sectional area changes smoothly so that the enlargement angle is small, are of practical importance. Due to the reduction of the curvature of the duct the onset of recirculation is delayed. The objective of this paper is to determine the reattachment length as a function of the inlet velocity, for a duct with a curvature that is reduced by decreasing the enlargement angle so that the cross-sectional area changes smoothly along the axial direction.

2. Model Equations

The two-dimensional, steady-state, incompressible, viscous flow is governed by the conservation of mass and the laws of motion, and is described by the following well-known equations

$$\frac{\partial u}{\partial x} + \frac{\partial v}{\partial y} = 0 \tag{1}$$

$$u\frac{\partial u}{\partial x} + v\frac{\partial u}{\partial y} = -\frac{1}{\rho}\frac{\partial p}{\partial x} + \nu\left\{\frac{\partial^2 u}{\partial x^2} + \frac{\partial^2 u}{\partial y^2}\right\} \tag{2}$$

$$u\frac{\partial v}{\partial x} + v\frac{\partial v}{\partial y} = -\frac{1}{\rho}\frac{\partial p}{\partial y} + \nu\left\{\frac{\partial^2 v}{\partial x^2} + \frac{\partial^2 v}{\partial y^2}\right\}. \tag{3}$$

Here u is the component of velocity in the x-direction and correspondingly v in y-direction, p is the pressure, ρ is the mass density and ν is the kinematic viscosity of the fluid (air in this case). The geometry of the flow channel and the boundary conditions are shown in Fig. 1. A linear velocity profile is assumed at the inlet of the flow channel. On the surface of the channel the no-slip boundary condition $u = v = 0$ is applied. This is further elaborated in the following sections. The exit of the channel is left free, i.e., no boundary condition is imposed but the equations of motion are applied in the vorticity-stream function form.

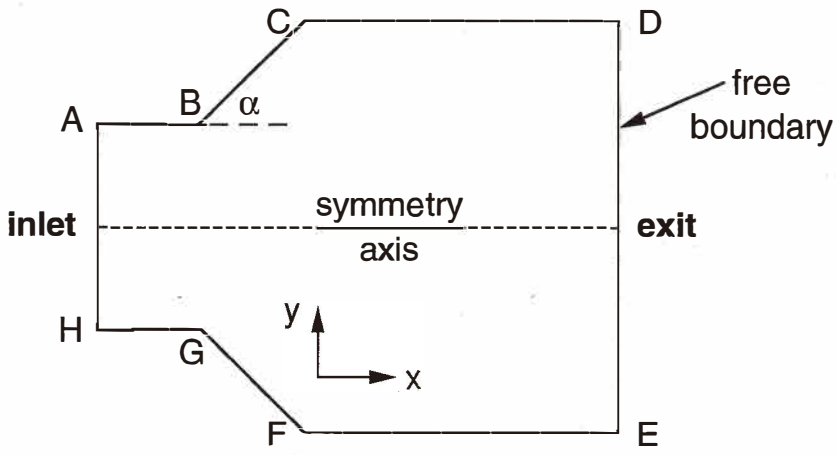

Fig. 1. Geometry for duct. AH denotes the inlet, DE the exit, α the enlargement angle, and ABCD and EFGH are no-slip boundaries ($u = v = 0$).

Since the geometry is symmetric with respect to the center-line (referred to as the symmetry axis in Fig. 1) of the channel, the simulation has been confined to the upper portion of the flow channel and the symmetry boundary conditions are implemented on the center-line.

The number of unknown variables can be reduced to two by casting the governing equations in the vorticity-stream function formulation. The stream function ψ is defined as

$$u = \frac{\partial \psi}{\partial y}, v = -\frac{\partial \psi}{\partial x} \tag{4}$$

so that the mass conservation equation is satisfied automatically. Defining the vorticity ω as

$$\omega = \frac{\partial v}{\partial x} - \frac{\partial u}{\partial y} \tag{5}$$

eqs. (1)–(3) become

$$\frac{\partial^2 \psi}{\partial x^2} + \frac{\partial^2 \psi}{\partial y^2} = -\omega \tag{6}$$

$$u\frac{\partial \omega}{\partial x} + v\frac{\partial \omega}{\partial y} = v\left\{\frac{\partial^2 \omega}{\partial x^2} + \frac{\partial^2 \omega}{\partial y^2}\right\}. \tag{7}$$

The boundary conditions have to be suitably applied in terms of the stream function and the vorticity.

3. Numerical Method

The governing equations (6) and (7) are discretized using the rotated finite difference scheme.[10] The nodal connectivity for an interior node, I, is shown in Figs. 2(a) to 2(d), where N_1, N_2, N_3, ... N_8 are the surrounding nodes. For purposes of discretization, the vorticity transport equation (7) is recast in the form

$$\sqrt{u^2 + v^2}\,\frac{\partial \omega}{\partial s} = \nu\left\{\frac{\partial^2 \omega}{\partial x^2} + \frac{\partial^2 \omega}{\partial y^2}\right\}$$

where $\frac{\partial \omega}{\partial s}$ is the stream derivative of ω in the direction of the streamline given by

$$\frac{dx}{u} = \frac{dy}{v}.$$

The streamline, IP (where P is an arbitrary point denoting the intersection of the local streamline with the boundary of the cell) is assumed to be linear within the cell connecting the eight surrounding nodes. The various possible choices for P are shown in Figs. 2(a) to 2(d). The stream derivative $\frac{\partial \omega}{\partial s}$ at I, for all the possible choices shown, is then discretized by

$$\frac{\partial \omega}{\partial s} = \frac{\omega(I) - \omega(P)}{d_{IP}} \tag{8}$$

where d_{IP} is the distance between I and P. When the streamline does not coincide with the coordinates axes, P has to be interpolated between the neighboring nodes and this can be done in many ways. In this work, a linear interpolation is employed. When the interior node is near the boundary, there will not be eight neighboring nodes if the domain is not rectangular, and $\omega(P)$has to be interpolated accordingly. When the velocity vector is in the direction of one of the coordinate axes, the scheme reduces to the usual first-order upwinding. This discretization results in a marginally diagonally dominant discrete set of equations. The scheme is closely related to the skew-upstream differencing technique of Raithby[11] but the diagonal dominance for the latter cannot be guaranteed. In many respects the discretization employed here is along the lines proposed by Rice and Schnipke[12] but differs in the interpolation of point P. The diffusive operator is discretized by

$$\frac{\partial^2 \omega}{\partial x^2} = \frac{d_{08}\omega_4 - (d_{08} + d_{04})\omega_I + d_{04}\omega_8}{\frac{d_{04}d_{08}(d_{04} + d_{08})}{2}} \tag{9}$$

$$\frac{\partial^2 \omega}{\partial y^2} = \frac{d_{02}\omega_6 - (d_{06} + d_{02})\omega_I + d_{06}\omega_2}{\frac{d_{02}d_{06}(d_{02} + d_{06})}{2}} \tag{10}$$

where d_{02}, d_{04}, d_{06} and d_{08} are the distances of the nodes N_2, N_4, N_6 and N_8 from node I, respectively.

Poisson's equation for the stream function and the transport equation for the vorticity are decoupled and solved as follows.

(1) Assuming an initial estimated vorticity distribution ω^0, Poisson's equation

$$\frac{\partial^2 \psi}{\partial x^2} + \frac{\partial^2 \psi}{\partial y^2} = -\omega^0$$

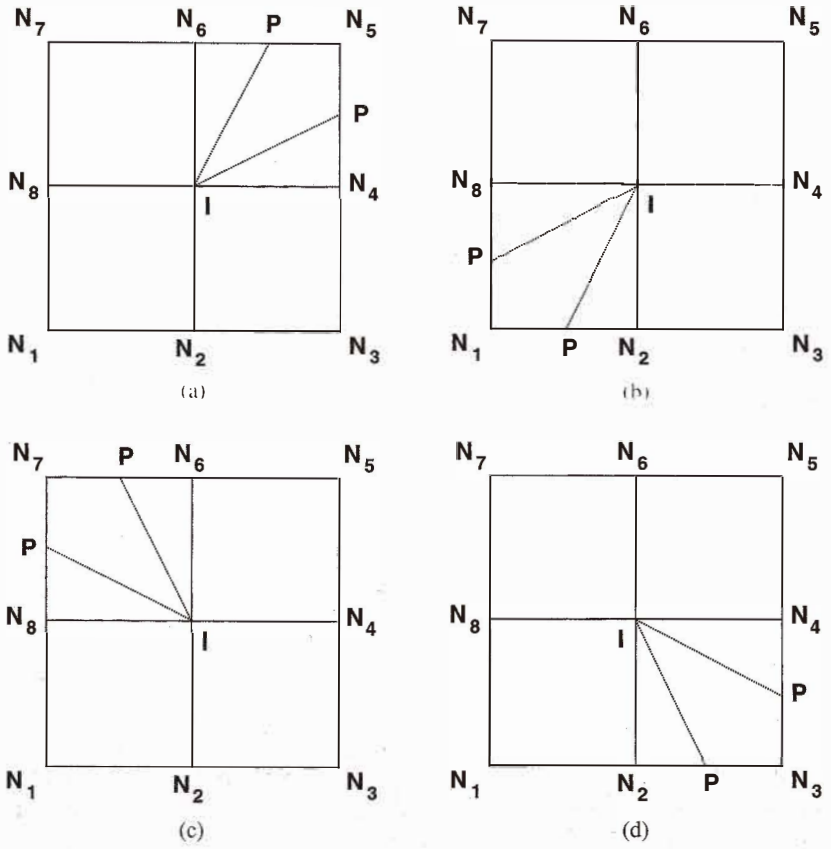

Fig. 2. Nodal connectivity for the interior node I for (a) $u \leq 0$ and $v \leq 0$, (b) $u \geq 0$ and $v \leq 0$, (c) $u \geq 0$ and $v \geq 0$, (d) $u \leq 0$ and $v \geq 0$. The two possible positions of P shown depend on the relative magnitudes of u and v.

is solved along with the boundary condition for ψ to obtain a new ψ^1. A linear velocity profile is assumed at the inlet of the duct, and on the surface of the channel ψ is set to zero. At the exit of the channel, Poisson's equation for the stream function is applied as a boundary condition.

(2) With the available stream function distribution ψ^1, the velocity components at nodes are calculated from

$$u = \frac{\partial \psi^1}{\partial y}, v = -\frac{\partial \psi^1}{\partial x}.$$

(3) With the calculated velocity distribution, the vorticity transport equation

$$\sqrt{u^2 + v^2}\,\frac{\partial \omega}{\partial s} = \nu\left\{\frac{\partial^2 \omega}{\partial x^2} + \frac{\partial^2 \omega}{\partial y^2}\right\}$$

is solved along with the 'updated' boundary condition for the vorticity to obtain a new w^1. On the surface of the channel, the vorticity is unknown and it has to be calculated as a part of the iterative procedure. This wall vorticity is the source of disturbance and is advected and diffused at the interior fluid points. However, we are given only the no-slip boundary conditions for the velocity components. Noting that the governing nonlinear equations are coupled and of the fourth order in stream function, the vorticity on the no-slip boundary can be calculated consistently with Poisson's equation for the stream function. An excellent detailed treatment of this boundary condition is elucidated by Roache in his book[3] and in another related article[13] but it corresponds to the pressure boundary condition. On the no-slip boundary $\frac{\partial^2 \psi}{\partial s^2} = 0$, where s is a direction vector along the boundary and the vorticity,

$$\omega = -\frac{\partial^2 \psi}{\partial n^2}$$

where n is a unit normal to the boundary, can be calculated consistently with the no-slip boundary condition.

A remark must be made regarding the previously mentioned free boundary condition for the stream function and the vorticity. There has been significant interest[14,15] in determining an optimal open boundary condition at the 'exit' so as to reduce computational requirements. Sani and Gresho[15] gave a detailed resume of all boundary conditions at the free boundary; however, there appears to be no unanimous answer. In our calculations the vorticity transport equation itself, in the absence of any other information, is applied as a condition on the boundary.

(4) Steps (1) to (3) are repeated until convergence is achieved. As is well known, it is crucial to under-relax the flow variables during the iteration cycle particularly for flows with high Reynolds number to avoid divergence.

4. Results and Discussion

In order to test and validate the accuracy of the numerical solutions, the scheme has been applied to extreme or limiting conditions, such as pure diffusion and pure convection, for which the analytical solutions are known. In the pure convection case with a known velocity along the diagonals of the unit cell, the scheme was able to predict the exact solution even when the analytical solution was discontinuous across the diagonal. Similarly, for the pure diffusion case, the scheme was able to predict the exact vorticity distribution, biquadratic in x and y when there was no flow.

The flow inside the channel, besides the inlet velocity and the kinematic viscosity of the liquid, depends on three geometrical quantities: enlargement angle α, the duct depth DE and duct length FE (Fig. 1). The numerical values for these quantities are $HG = 10$ cm, $GF \cos \alpha = 40$ cm, $FE = 200$ cm, $GF \sin \alpha = 4$ cm, $DE = 10$ cm and $\alpha = 5.7$ degrees. The kinematic viscosity of air is taken to be $\nu = 0.1785$ cm^2/s and the Reynolds number is varied by increasing the inlet velocity. A nonuniform grid has been employed.

In the numerical experiments we have considered, because of the small enlargement angle, there is no vortex formation even for high Reynolds numbers ($R_e \leq 400$), for the given characterisitic length $DE/2$. Figure 3 depicts streamlines for an inlet velocity of 10 cm/s. Because of the relatively small velocity and the given duct geometry, we observe no vortex formation and the reattachment length is virtually zero. At higher velocities, 30 cm/

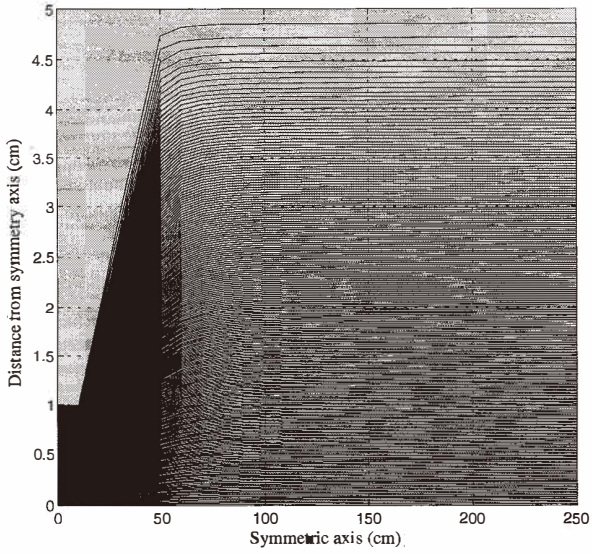

Fig. 3. Streamlines in the flow channel for an inlet velocity of 10 cm/s.

s and 1 m/s, a vortex forms (Figs. 4 and 5) and moves downstream as the inlet velocity is increased, thus increasing the reattachment length. The width of the vortex region increases with the Reynolds number. The reattachment length measured along the axis of the duct from point B (Fig. 1), and normalized to $DE/2$, is shown as a function of the inlet velocity (Fig. 6). The reattachment length for low velocities (low Reynolds numbers) varies linearly with the Reynolds number.

5. Conclusion

A numerical method, taking into account the local nature of the streamline, has been presented to predict the nature of the flow in a channel with a small enlargement angle. Numerical solutions are obtained for a range of inlet velocities from 1 cm/s to 1 m/s. For this range of velocities considered, the vortices start to form only when inlet velocity is 20 cm/s or higher and it is observed that the reattachment length varies almost linearly with the velocity. For higher values of the enlargement angle, the formation of the vortex region is almost immediate even for extremely low Reynolds numbers and computational requirements in terms of iterations dramatically increase as the enlargement angle increases.

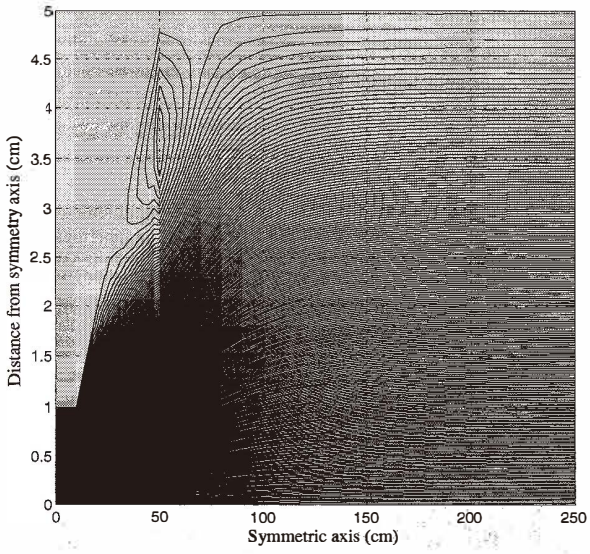

Fig. 4. As in Fig. 3 but for an inlet velocity of 30 cm/s.

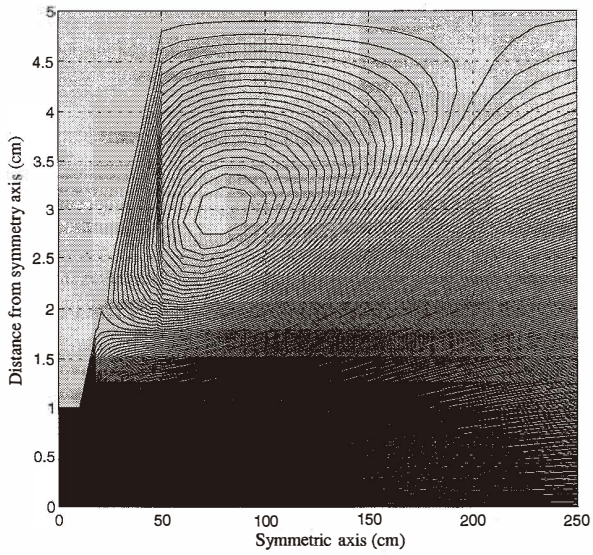

Fig. 5. As in Fig. 3 but for an inlet velocity of 1 m/s.

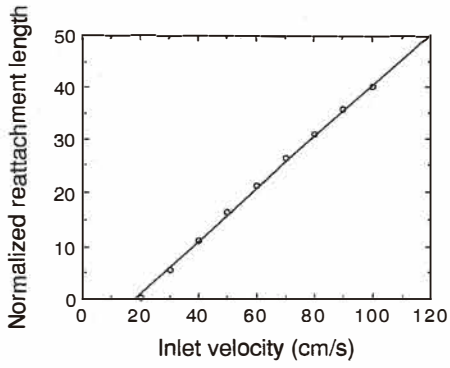

Fig. 6. The normalized reattachment length as a function of inlet velocity.

Acknowledgments

The authors wish to thank Dr. N. R. Swart, NOI, Quebec City, Canada for stimulating discussions. This work was supported by the Natural Sciences and Engineering Research Council (NSERC) of Canada and Yamatake-Honeywell Co., Ltd., Japan.

References

1 R. G. Johnson, R. E. Higashi, P. J. Bohrer and R. W. Gehman: Proc. Int. Conf. Solid-State Sensors and Actuators (Philadelphia, USA, June 11-14, 1985) p. 358.
2 C. H. Mastrangelo and P.S. Muller: Technical Digest, IEEE Solid-State Sensor and Actuator Workshop (Hilton Head Island, South Carolina, 1988) p. 43.
3 P. J. Roache: Computational Fluid Dynamics (Hermosa, Albuquerque, 1976).
4 R. T. Peyret and T. D. Taylor: Computational methods for fluid flow (Springer-Verlag, New York, 1983).
5 S. V. Patankar: Numerical heat transfer and fluid flow (Hemisphere Publishing Co., New York, 1980).
6 K. Morgan, J. Periaux and F. Thomasset (eds.): A GAMM Workshop, Notes on numerical fluid dynamics (Friedr. Vieweg Son, Braunschweig, 1984).
7 S. C. R. Dennis and Go-Zo Chang: Jl. Fluid Mech. **42** (1970) 471.
8 A. E. Hamielec and J. D. Raal: Physics of Fluids **12** (1969) 11.
9 A. Acrivos, L.G. Leal, D. D. Snowden and F. Pan: Jl. Fluid Mech. **34** (1970) 25.
10 D. Thangaraj, H. Wu and S. Jayaram: Proceedings of the 1994 IEEE-IAS 27th meeting (Denver, Colorado) p. 1676.
11 G. D. Raithby: Comp. Methods in Applied Mechanics and Engineering **9** (1976) 153.
12 J. G. Rice and R. J. Schnipke: Comp. Methods in Applied Mechanics and Engineering **48** (1985) 313.
13 P. J. Roache: Int. Journal for Numerical Methods in Fluids **8** (1988) 1459.
14 P. M. Gresho and R. L. Sani: Int. Journal for Numerical Methods in Fluids **11** (1990) 951.
15 R. L. Sani and P. M. Gresho: Int. Journal for Numerical Methods in Fluids **18** (1994) 983.